Biped Gait Generation and Control Based on a Unified Property of Passive Dynamic Walking

Fumihiko Asano, Zhi-Wei Luo, and Masaki Yamakita

***Abstract*—Principal mechanisms of passive dynamic walking are studied from the mechanical energy point of view, and novel gait generation and control methods based on passive dynamic walking are proposed. First, a unified property of passive dynamic walking is derived, which shows that the walking system's mechanical energy increases proportionally with respect to the position of the system's center of mass. This yields an interesting indeterminate equation that determines the relation between the system's control torques and its center of mass. By solving this indeterminate equation for the control torque, active dynamic walking on a level can then be realized. In addition, the applications to the robust energy referenced control are discussed. The effectiveness and control performances of the proposed methods have been investigated through numerical simulations.**

***Index Terms*—Biped robots, passive dynamic walking, gait generation, limit cycles, legged locomotion, mechanical energy.**

I. Introduction

Since the successive development of humanoid robots by Honda, various biped robots have been published one after another by manufacturing industries. Nowadays, it seems as if the robot's walking control technology has reached almost the stage of completion and the biped walking control technique is never difficult. The central problem of biped locomotion is shifted recently to how to create beauty and effectiveness in the robot's walking gait.

Many studies have reported so far on the gait optimization problem with respect to (w.r.t.) the system's energy consumption, however, definitions and opinions on the optimality are quite different. The unified concept has yet been established since there aren't any models which can exhibit an optimal gait. McGeer's passive dynamic walking [9] has been considered to be a clue to elucidate this problem, and recently some control laws and mechanical structure designs which are conscious of passive dynamic walking mechanisms have been proposed. Passive dynamic walking closely relates to *dynamics based control* (DBC), which suggests an ultimate analysis for the gait generation problem w.r.t. energy consumption. Energy tracking control proposed by Goswami *et al.* [4] is known as the first application of a passive dynamic walking mechanism to active dynamic walking on a level. Although this method cannot be called practical from the zero moment point (ZMP) point of view (see [1]), the suggestion of the mechanical energy restoration concept is very important and this leads to the work by Spong [15] and Asano *et al.* [1], [2]. These works are based on the concept that mechanical energy restoration which dissipates at every heel-strike instant is a necessary condition common to all dynamic gait generation. Self-excited walking proposed by Ono *et al.* [10], [11] and ballistic walking by van der Linde [8] are also interesting approaches by under-actuated mechanism. The studies by Kajita *et al.* [7] and Sano and Furusho [14] focused on global physical quantities such as mechanical energy and angular momentum. Although it is very difficult to define the *naturalness* of gait and its explanations are different according to researchers, the common target of all of these works is to find a dynamic gait which achieves the longest movable distance with the shortest time by the same energy supply. Most of the previous works emphasize the energy efficiency based on their own results. None of them, however, clarified the problems on what the maximum efficiency is at all. It is necessary to compare the control performances systematically and objectively.

Manuscript received March 29, 2004; revised July 22, 2004. This paper was recommended for publication by Associate Editor W. Chung and Editor H. Arai upon evaluation of the reviewers' comments. This paper was presented at the 6th International Conference on Climbing and Walking Robots, Catania, Italy, September 2003.

F. Asano and Z.-W. Luo are with Biomimetic Control Research Center, The Institute of Physical and Chemical Research (RIKEN), Nagoya 463-0003, Japan (e-mail: asano@bmc.riken.jp).

M. Yamakita is with the Department of Mechanical and Control Systems Engineering, Graduate School of Science and Engineering, Tokyo Institute of Technology, Tokyo 152-8552, Japan.

Digital Object Identifier 10.1109/TRO.2005.847610

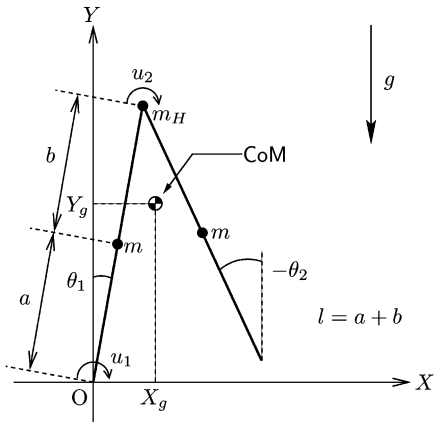

Fig. 1. Model of the compass-gait biped.

Based on the above observations, in this paper, we reconsider the principal gait generation mechanisms of passive dynamic walking from the point of view of the system's mechanical energy. We derive a partial differential equation which characterizes a unified property of passive dynamic walking. This property shows the principle relation between the system's energy change and its center of mass (CoM). We then formulate and define the gait generation problem as a solution of an indeterminate equation related to the partial differential equation. We also show that our previous works [1], [2] are special examples within this unified framework. In addition, we propose a robust control law using a reference mechanical energy trajectory. By using a global physical quantity, we can make the walking system robust without introducing any desired time trajectories of angular positions nor velocities. Although the exact definition of DBC is also very difficult, control approaches based on "trajectory-free" and "autonomous," i.e., "time-independent," are important for naturalness of gait and can be considered the key concepts of DBC. The validity of the proposed method is investigated through numerical simulations. Furthermore, analysis of the control performances of energy efficiency and robust stability is numerically performed by introducing some criterion functions. Based on the results, we theoretically clarify the problems on what the maximum efficiency is and what its necessary condition is. Throughout these studies, we suggest that, the dynamic bipedal walking cannot be realized by only applying the existing control theory but depends mainly on the deep understanding of the complex physical characteristics of the mechanical system.

II. Model of the Compass-Gait Biped

This paper deals with a full-actuated planar compass-like biped robot shown in Fig. 1. Note that there exits a foot link whose thickness and mass can be ignored, and the ankle joint torque u_1 can be occurred relative to it. The model equations and its basic features are described in the following.

A. Dynamic Equations

The dynamic equation of the biped robot during the swing phase is given as

$$\boldsymbol{M}(\boldsymbol{\theta})\ddot{\boldsymbol{\theta}} + \boldsymbol{C}(\boldsymbol{\theta},\dot{\boldsymbol{\theta}})\dot{\boldsymbol{\theta}} + \boldsymbol{g}(\boldsymbol{\theta}) = \boldsymbol{S}\boldsymbol{u} \tag{1}$$

where $\boldsymbol{\theta} = [\theta_1 \ \theta_2]^T$ is the angle vector in the configuration space as defined in Fig. 1, and we choose them as relative angles w.r.t. the vertical Y direction. The details of the matrices in (1) are as follows:

$$\boldsymbol{M}(\boldsymbol{\theta}) = \begin{bmatrix} m_H l^2 + ma^2 + ml^2 & -mbl\cos(\theta_1-\theta_2) \\ -mbl\cos(\theta_1-\theta_2) & mb^2 \end{bmatrix}$$

$$\boldsymbol{C}(\boldsymbol{\theta},\dot{\boldsymbol{\theta}}) = \begin{bmatrix} 0 & -mbl\sin(\theta_1-\theta_2)\dot{\theta}_2 \\ mbl\sin(\theta_1-\theta_2)\dot{\theta}_1 & 0 \end{bmatrix}$$

$$\boldsymbol{g}(\boldsymbol{\theta}) = \begin{bmatrix} -(m_H l + ma + ml)\sin\theta_1 \\ mb\sin\theta_2 \end{bmatrix} g$$

$$\boldsymbol{S}\boldsymbol{u} = \begin{bmatrix} 1 & 1 \\ 0 & -1 \end{bmatrix} \begin{bmatrix} u_1 \\ u_2 \end{bmatrix}.$$

We assume that the inertia of the links and viscosity of the joints can be ignored and define the whole mass of the robot as

$$M := m_H + 2m. \tag{2}$$

By setting the tip of the stance leg as the origin of the coordinate as shown in Fig. 1, the horizontal position of the CoM X_g is expressed as

$$X_g = \frac{(m_H l + ma + ml)\sin\theta_1 - mb\sin\theta_2}{M}. \tag{3}$$

In this paper, we call X_g simply CoM, and the origin O is switched to the tip of the stance leg at every just after transition instant.

The physical parameters of the robot in all of the following numerical simulations are chosen as $m_H = 10.0, m = 5.0$ kg, $a = 0.5, b = 0.5$ and $l = a + b = 1.0$ m, respectively.

B. Transition Equations

The collision between the swing leg and floor is assumed to be perfectly inelastic. In this case, since the stance and swing leg changes each other instantly, there exist no double support phase. Following the law of conservation of angular momentum, we can obtain a simple transition equation of the angular velocity as

$$\boldsymbol{Q}^+(\alpha)\dot{\boldsymbol{\theta}}^+ = \boldsymbol{Q}^-(\alpha)\dot{\boldsymbol{\theta}}^- \tag{4}$$

where $\dot{\boldsymbol{\theta}}^-$ and $\dot{\boldsymbol{\theta}}^+$ denote just before and after angular velocity, respectively. Please see [1] for the details of the matrices $\boldsymbol{Q}^+$ and $\boldsymbol{Q}^-$. α [rad] is the half inter-leg angle at the transition instant and is given by

$$\alpha = \frac{\theta_1^- - \theta_2^-}{2} = \frac{\theta_2^+ - \theta_1^+}{2} > 0. \tag{5}$$

C. Mechanical Energy

The mechanical energy E of the robot is defined as

$$E(\boldsymbol{\theta},\dot{\boldsymbol{\theta}}) = \frac{1}{2}\dot{\boldsymbol{\theta}}^T\boldsymbol{M}(\boldsymbol{\theta})\dot{\boldsymbol{\theta}} + P(\boldsymbol{\theta}) \tag{6}$$

where $P(\boldsymbol{\theta})$ is the potential energy with the tip of the stance leg as a standard and is given by

$$P(\boldsymbol{\theta}) = \{(m_H l + ma + ml)\cos\theta_1 - mb\cos\theta_2\}g. \tag{7}$$

Time derivative of the mechanical energy yields

$$\dot{E} = \dot{\boldsymbol{\theta}}^T\boldsymbol{S}\boldsymbol{u} = \dot{\theta}_1 u_1 + (\dot{\theta}_1 - \dot{\theta}_2)u_2. \tag{8}$$

III. Passive Dynamic Walking Mechanism and Its Application to Active Walking on a Level

This section considers the essence of passive dynamic walking and describes its applications to active dynamic walking on a level.

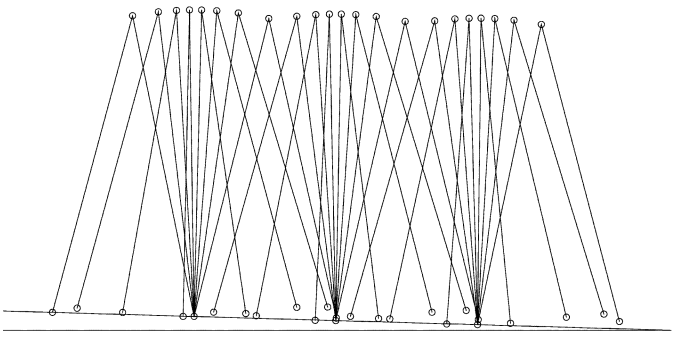

Fig. 2. Passive dynamic walking on a slope.

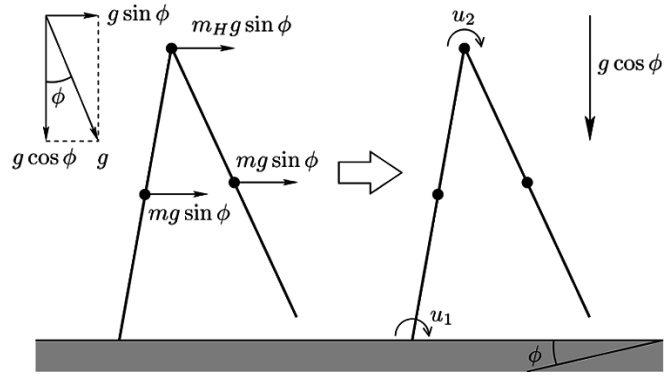

Fig. 3. Passive dynamic walking mechanism.

A. Analysis of Passive Dynamic Walking Mechanism

The compass-gait biped robot shown in Fig. 1 can walk down on a gentle slope from a suitable initial condition without any actuation as shown in Fig. 2. Note that the *foot-scuffing* during the single support phase is ignored. This style can be considered an *ultimate walking motion* from the energy consumption point of view, and this is also an *ultimate DBC*. By applying the passive dynamic walking mechanism to gait synthesis of biped robots, it is expected that natural and energy-effective active dynamic walking on a level can be realized. Some related studies have been reported so far. As an advanced study, energy tracking control proposed by Goswami *et al.* is especially excellent [4]. This is realized by tracking control for a constant reference energy which is obtained in passive dynamic walking on a gentle slope. By using this method, a stable limit cycle on a level can be generated; however, some essential factors such as torque pattern become dramatically different from those of original passive dynamic walking. For further discussion, the reader is referred to [1]. We must be careful to reproduce the principal mechanism of passive dynamic walking on the horizontal plane without destroying its properties.

As shown in Fig. 3 (left), dividing the nominal gravity g into tangential element to the slope $g\sin\phi$ and normall one $g\cos\phi$, the tangential element is found to act as a driving force for the robot. By regarding this as an *active* walking on a level as shown in Fig. 3 (right), the robot seemed to be driven by the following equivalent transformed torque:

$$\boldsymbol{S}\boldsymbol{u}_\phi = \begin{bmatrix} (m_H l + ma + ml)\cos(\theta_1 - \phi) \\ -mb\cos(\theta_2 - \phi) \end{bmatrix} g\sin\phi \tag{9}$$

in the *virtual* gravity field whose magnitude is $g\cos\phi$. Note that, in this case, the angles are also chosen w.r.t. the vertical Y direction in Fig. 1; see the Appendix for details.

The mechanical energy in the gravity condition of Fig. 3 (right) can be defined as

$$E_\phi(\boldsymbol{\theta},\dot{\boldsymbol{\theta}}) = \frac{1}{2}\dot{\boldsymbol{\theta}}^T\boldsymbol{M}(\boldsymbol{\theta})\dot{\boldsymbol{\theta}} + P_\phi(\boldsymbol{\theta}) \tag{10}$$

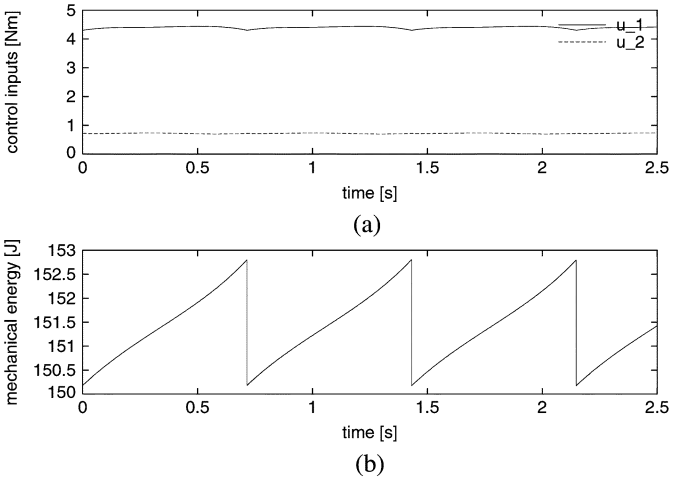

Fig. 4. Simulation results of passive dynamic walking where $\phi = 0.03$ rad. (a) Control inputs. (b) Mechanical energy E_ϕ.

where $P_\phi(\boldsymbol{\theta})$ is the virtual potential energy determined as

$$P_\phi(\boldsymbol{\theta}) = \{(m_H l + ma + ml)\cos(\theta_1 - \phi) - mb\cos(\theta_2 - \phi)\} g \cos\phi. \quad (11)$$

This can be obtained by replacing the angles $\theta_1 \to \theta_1 - \phi, \theta_2 \to \theta_2 - \phi$, and gravity: $g \to g\cos\phi$ in (7), respectively.

Fig. 4 shows the simulation results of passive dynamic walking on a gentle slope whose angle is 0.03 rad. From Fig. 4(a), as can be expected from (9), we can see that flat control torques are generated, and, from Fig. 4(b), the mechanical energy is restored monotonically during the single support phase.

The *constant-like* torques can be considered *the symbol of unconsciousness*. On the other hand, the impulsive transition feature, without double-support phase, can be intuitively regarded as a *vigor* for fast and energy-effective walking. In order to get the *vigor*, the walking robot must store the mechanical energy effectively and exchange the support leg with the impulsive and inelastic heel-strike collision instantaneously. These two features can be considered indicators of natural and effective walking motion. Based on the observations, in the following we describe the gait generation methods proposed so far.

B. Virtual Passive Dynamic Walking

As the most intuitive method imitating the mechanism of passive dynamic walking, we have proposed virtual passive dynamic walking using a small artificial gravity called "virtual gravity" to the walking direction [2]. Active dynamic walking can be realized via equivalent torque transformation of the virtual gravity effect, as shown in Fig. 5. The equivalent transformed torque is given by

$$\boldsymbol{S}\boldsymbol{u}_{\rm vg} = \begin{bmatrix} (m_H l + ma + ml)\cos\theta_1 \\ -mb\cos\theta_2 \end{bmatrix} g\tan\phi. \quad (12)$$

See the Appendix for the detailed derivations.

Fig. 6 shows the simulation results of virtual passive dynamic walking on a level where the walking speed is 0.60 m/s and $\phi = 0.0265$ rad. We can see that the shape of torque and mechanical energy are quite similar to those of original passive dynamic walking. Spong has also proposed an energy shaping control approach [15]; however, in our virtual gravity approach, the control inputs are more flat than his results. This property is very important from the ZMP regulation point of view.

This method can generate a dynamic gait very easily, however, since the control input is determined by (12) uniquely, arbitrary manipulation of some important factors such as ZMP cannot be performed. As a solution to this problem, another method has been proposed and is described in the following.

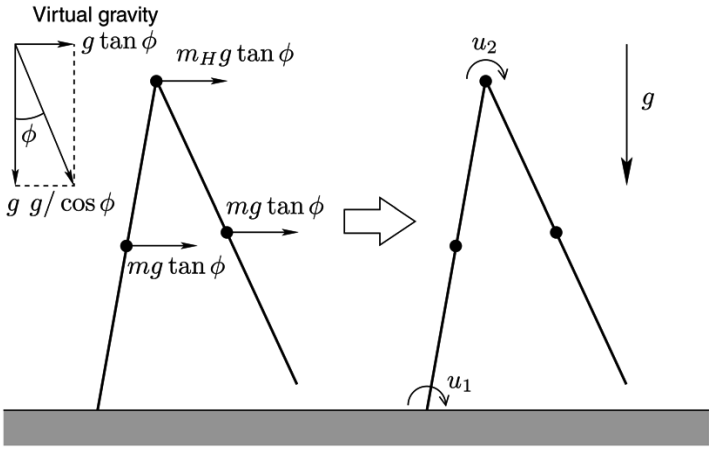

Fig. 5. Virtual passive dynamic walking mechanism.

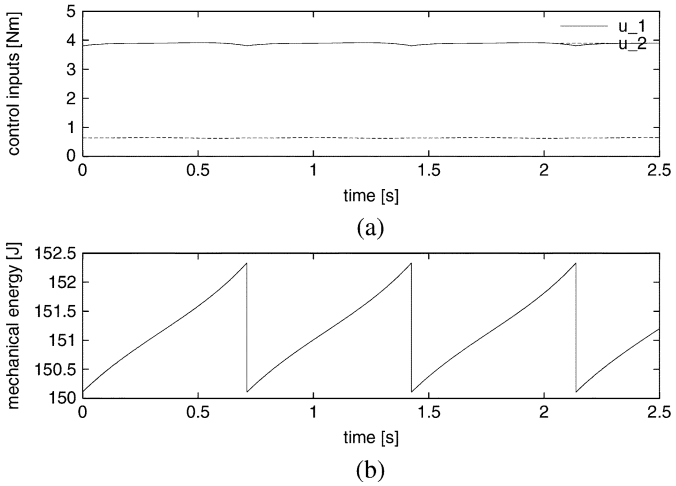

Fig. 6. Simulation results of virtual passive dynamic walking where $\phi = 0.0265$ rad. (a) Control inputs. (b) Mechanical energy.

C. Energy Constraint Control

As another gait generation method based on passive dynamic walking, we have considered the imitation of mechanical energy restoration. Letting λ be a positive constant, we consider the following condition:

$$\dot{E} = \dot{\boldsymbol{\theta}}^T \boldsymbol{S}\boldsymbol{u} = \lambda. \quad (13)$$

By solving (13) for the control input $\boldsymbol{u}$ in real time, the mechanical energy can be restored monotonically. We call this approach "Energy Constraint Control" [1]. The detail of (13) is written as

$$\dot{\theta}_1 u_1 + (\dot{\theta}_1 - \dot{\theta}_2) u_2 = \lambda \quad (14)$$

which is an indeterminate equation with two unknown variables u_1 and u_2. Therefore, the energy constraint control problem yields how to solve (14) for the control inputs u_1 and u_2 in real time. As a basic algorithm, this section introduces a solution using a constant torque ratio. We choose the torque constraint condition as

$$u_1 = \mu u_2 \quad (15)$$

and, by substituting (15) into (14), we obtain the control input as

$$\boldsymbol{S}\boldsymbol{u} = \begin{bmatrix} \mu + 1 \\ -1 \end{bmatrix} \frac{\lambda}{(\mu+1)\dot{\theta}_1 - \dot{\theta}_2}. \quad (16)$$

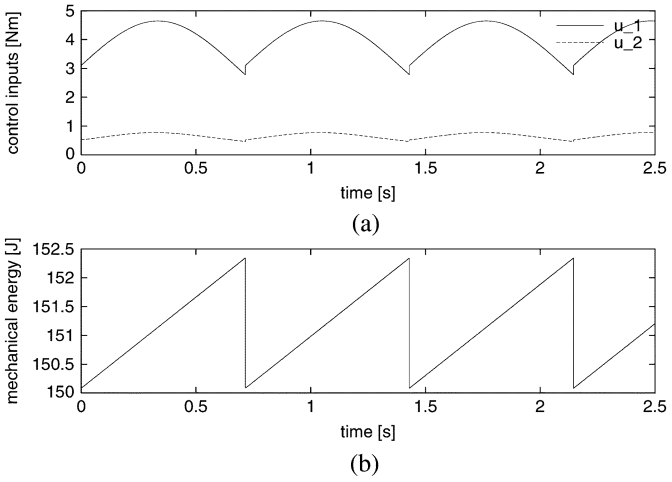

Fig. 7. Simulation results of dynamic walking by energy constraint control where $\lambda = 3.16$. (a) Control inputs. (b) Mechanical energy.

In the case of virtual passive dynamic walking, following (12), the torque ratio yields

$$\frac{u_1}{u_2} = \frac{(m_H l + ma + ml)\cos\theta_1}{mb\cos\theta_2} - 1. \tag{17}$$

By approximating this around the equilibrium point, we can obtain the *nominal* torque ratio as

$$\mu = \frac{m_H l + ma + ml}{mb} - 1 = 6.0.$$

Fig. 7 shows the simulation results of active dynamic walking on a level by energy constraint control using the approximated constant torque ratio where the walking speed is 0.60 m/s and $\lambda = 3.16$. This method is superior in the sense that the gait can be generated by only selecting of λ and μ, and the ZMP can also be manipulated arbitrarily by controlling the ankle torque. However, rationality of the constraint condition of (13) is not clear. Based on the observations, in Section IV, we will investigate the energy restoration mechanism more strictly.

IV. Formulation of the Gait Generation Problem

Based on the above studies, this section reconsiders the mechanical energy restoration mechanism more strictly and formulates the biped gait generation problem.

A. Energy Restoration Mechanism Revisited

Following (8) and (12), the mechanical energy restoration rate w.r.t. time yields

$$\begin{aligned}\dot{E} &= \dot{\boldsymbol{\theta}}^T \boldsymbol{S}\boldsymbol{u}_{\rm vg} \\ &= \dot{\boldsymbol{\theta}}^T \begin{bmatrix} (m_H l + ma + ml)\cos\theta_1 \\ -mb\cos\theta_2 \end{bmatrix} g\tan\phi \\ &= \{(m_H l + ma + ml)\dot{\theta}_1\cos\theta_1 - mb\dot{\theta}_2\cos\theta_2\} g\tan\phi \\ &= Mg\tan\phi\frac{d}{dt}\left\{\frac{(m_H l + ma + ml)\sin\theta_1 - mb\sin\theta_2}{M}\right\}. \end{aligned} \tag{18}$$

By taking into account (3), (18) can be rewritten as

$$\dot{E} = Mg\tan\phi\dot{X}_g. \tag{19}$$

Note that (19) is a reduction from a three-input–three-output relation $\boldsymbol{S}\boldsymbol{u} \rightarrow \dot{\boldsymbol{\theta}}$ of (8) to single-input–single-output (SISO) relation $Mg\tan\phi \rightarrow \dot{X}_g$, and this is achieved via concentration of the acceleration effect to the walking direction. In addition, following the relation

$$\frac{\partial E}{\partial X_g} = \frac{dE/dt}{dX_g/dt} \tag{20}$$

(19) can be transformed into

$$\frac{\partial E}{\partial X_g} = Mg\tan\phi \tag{21}$$

which suggests that there exits a homogeneous gravity element toward the walking direction, and this relation is always satisfied regardless of the existence of inertia moment and number of links [3]. Equation (21) concludes the results discussed so far because it includes the whole essential mechanisms of passive dynamic walking, energy restoration and gravity acceleration.

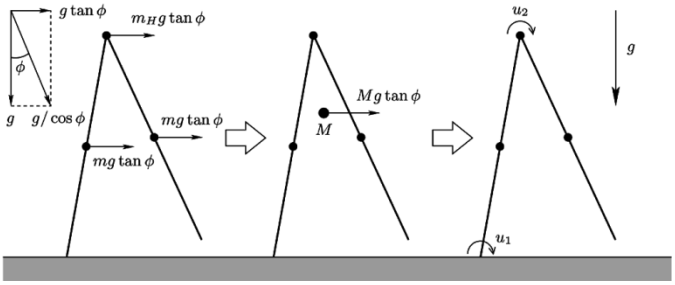

Fig. 8. Lumped virtual gravity-based dynamic walking mechanism.

B. Formulation

By defining the gait generation problem based on passive dynamic walking as *to obtain a solution* $\boldsymbol{u}$ *which satisfies the condition of* (21), from (8) and (19), it yields how to solve the following indeterminate equation:

$$\dot{\boldsymbol{\theta}}^T \boldsymbol{S}\boldsymbol{u} = Mg\tan\phi\dot{X}_g \tag{22}$$

for the control input $\boldsymbol{S}\boldsymbol{u}$ in real time or, in other words, how to divide the virtual gravity effect concentrated on the CoM to each joint torque as shown in Fig. 8. In this paper, we denote the solutions of (22) as $\boldsymbol{S}\boldsymbol{u}_{\rm vg}$ in the sense of reproducing the virtual gravity effect. We also call the gait generated by them as "virtual passive dynamic walking" uniformly.

In this section, as a method imitating the feature of passive dynamic walking, we consider a solution of (22) by constant torque ratio μ. The solution yields

$$\boldsymbol{S}\boldsymbol{u}_{\rm vg} = \begin{bmatrix} \mu + 1 \\ -1 \end{bmatrix} \frac{Mg\tan\phi\dot{X}_g}{(\mu+1)\dot{\theta}_1 - \dot{\theta}_2}. \tag{23}$$

We call this solution the "CTR formula." Fig. 9 shows the simulation results of active dynamic walking by CTR formula on a level where $\phi = 0.0265$ rad and $\mu = 6.0$. From the results, we can see that flatness of the control torque is realized, and thus we can conclude that it is very important whether or not CoM speed is included in the indeterminate equation.

C. General Solutions

Here, let us discuss general solutions of (22). Define the Jacobian of CoM $\boldsymbol{J}_X$ which satisfies

$$\dot{X}_g = \boldsymbol{J}_X(\boldsymbol{\theta})\dot{\boldsymbol{\theta}} \tag{24}$$

where

$$\boldsymbol{J}_X(\boldsymbol{\theta}) = \begin{bmatrix} M^{-1}(m_H l + ma + ml)\cos\theta_1 \\ -M^{-1}mb\cos\theta_2 \end{bmatrix}^T. \tag{25}$$

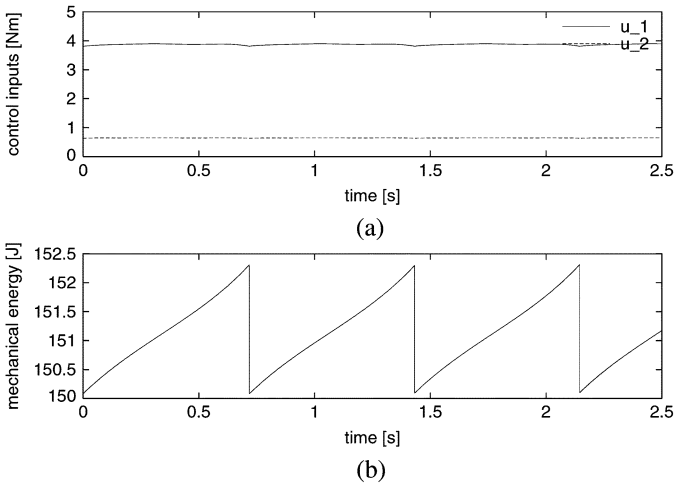

Fig. 9. Simulation results of dynamic walking by solution of (22) using a constant torque ratio where $\phi = 0.0265$ rad and $\mu = 6.0$. (a) Control inputs. (b) Mechanical energy.

By considering (24), (22) is equivalent to

$$\dot{\boldsymbol{\theta}}^T(\boldsymbol{Su} - Mg\tan\phi \boldsymbol{J}_X(\boldsymbol{\theta})^T) = 0. \tag{26}$$

Therefore, a general solution of (22) yields

$$\boldsymbol{Su}_{\rm vg} = Mg\tan\phi \boldsymbol{J}_X(\boldsymbol{\theta})^T + \left(\frac{\dot{\boldsymbol{\theta}}\dot{\boldsymbol{\theta}}^T}{\|\dot{\boldsymbol{\theta}}\|^2} - \boldsymbol{I}_2\right)\boldsymbol{\xi}. \tag{27}$$

The second term on the right-hand side of (27) is the null space of the solution and the vector $\boldsymbol{\xi} \in R^2$ is an arbitrary vector. The physical meaning of this term is not clear at present, and this paper does not investigate it. The first term on the right-hand side of (27) is equal to the equivalent transformed torque of the virtual gravity effect of (12). Therefore, the virtual gravity control is found to be the following basic solution of (22):

$$\boldsymbol{Su}_{\rm vg} = Mg\tan\phi \boldsymbol{J}_X(\boldsymbol{\theta})^T. \tag{28}$$

We call this solution the "CoMJ formula." In addition, as is clear from the comparison between (13) with (22), energy constraint control is a solution approximating the velocity of the CoM constant.

V. Robust Energy Control

Since the control formulation of (22) does not include any feedback factors for some reference trajectories, robust stability of the walking cycle is very weak as well as the original passive dynamic walking. Therefore, as a solution to this problem, this section proposes a reference energy trajectory tracking control utilizing the feature of mechanical energy behavior described in the previous section.

As described before, since the mechanical energy E changes w.r.t. X_g by a constant ratio, the desired energy trajectory E_d can be chosen as a linear function of X_g as follows:

$$E_d(X_g) = Mg\tan\phi X_g + E_0 \tag{29}$$

where E_0 J is the desired energy value when $X_g = 0$ in the steady motion, and this is determined uniquely according to ϕ. In this paper, the following asymptotic stabilizing control is proposed:

$$\frac{d}{dt}(E - E_d(X_g)) = -\zeta(E - E_d(X_g)) \tag{30}$$

where $\zeta > 0$ is the feedback gain. Following (8) and (29), time derivative of the energy tracking error yields

$$\frac{d}{dt}(E - E_d(X_g)) = \dot{\boldsymbol{\theta}}^T\boldsymbol{Su} - Mg\tan\phi\dot{X}_g. \tag{31}$$

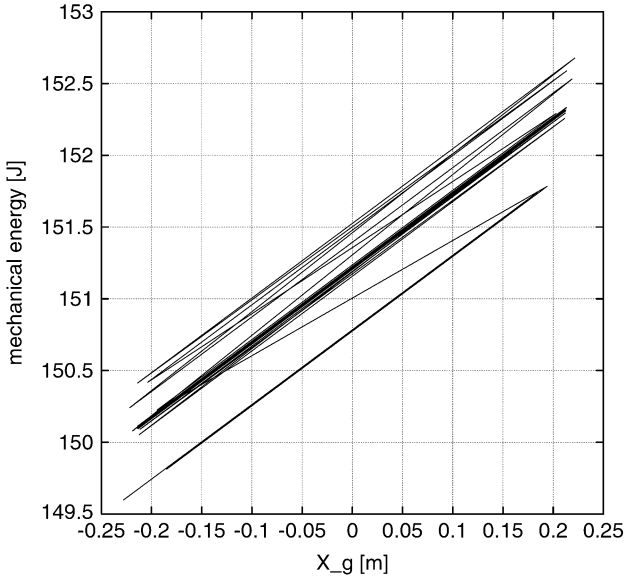

Fig. 10. Relationship between X_g and E where $\zeta = 0.0$.

Therefore, from (30) and (31), this control problem yields how to solve the following indeterminate equation:

$$\dot{\boldsymbol{\theta}}^T\boldsymbol{Su} = Mg\tan\phi\dot{X}_g - \zeta(E - E_d) \tag{32}$$

for the control input $\boldsymbol{Su}$ in real time. A solution of (32) for $\boldsymbol{\xi} = \boldsymbol{0}$ by constant torque ratio yields

$$\boldsymbol{Su}_{\rm vg} = \begin{bmatrix}\mu + 1\\ -1\end{bmatrix}\frac{Mg\tan\phi\dot{X}_g - \zeta(E - E_d)}{(\mu+1)\dot{\theta}_1 - \dot{\theta}_2}. \tag{33}$$

Note that the feedback system becomes autonomous here because the desired energy trajectory $E_d(X_g)$ is a function of X_g. This keeps the property of autonomy, i.e., time-independent, as passive dynamic walking approach.

Fig. 10 shows the simulation result of the CoM versus mechanical energy where $\phi = 0.0265$ rad, $\mu = 6.0$, and $\zeta = 0.0$. The robot starts walking from some initial condition close to the stable equilibrium point. In this case, the closed-loop walking system is equivalent to the one that is controlled by (23), and thus the gait converges to a stable limit cycle under the energy constraint condition of (21). Fig. 11 shows the results where $\zeta = 10.0$ and $E_0 = 151.210$ J. By the effect of the energy feedback control, the mechanical energy is stabilized to the desired energy trajectory. Fig. 12 shows the convergence of the step period where $\zeta = 0.0$ and 10.0, and we can confirm the control effectiveness. Fig. 13 shows the time evolution of the control inputs where $\zeta = 10.0$. The control inputs slide to *constant-like* ones as the gait converges to steady motion. Note that E_0 must be chosen correctly according to ϕ so that the torques become *constant-like* during steady walking. The detailed numerical analysis of the robust performance is performed in Section VI.

VI. Performance Analysis

In this section, by setting the control inputs as continuous-time signals, we exactly analyze the performances of the dynamic walking system and evaluate them using numerical simulations.

A. Robust Stability

In the previous section, robust energy control by CTR formula has been considered, whereas in this section we first consider the tracking

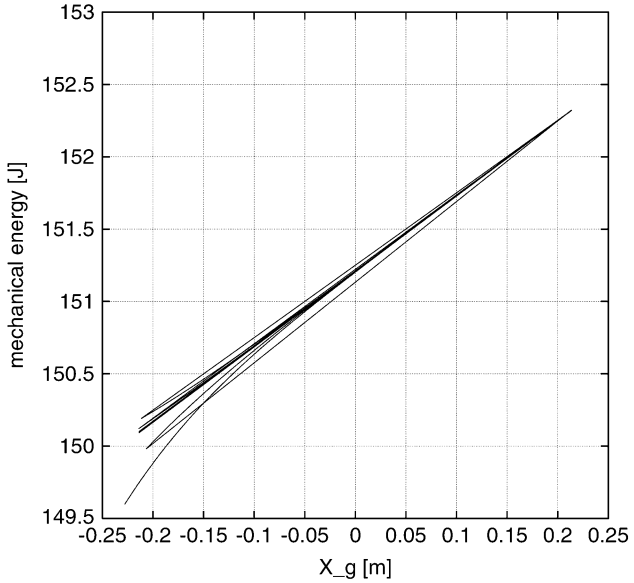

Fig. 11. Relationship between X_g and E where $\zeta = 10.0$.

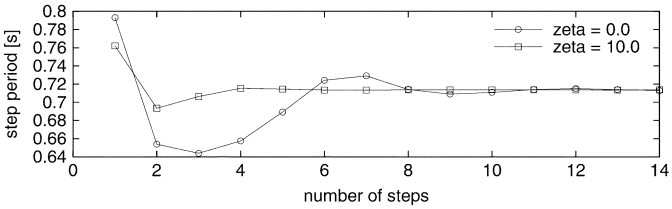

Fig. 12. Convergence of the step period.

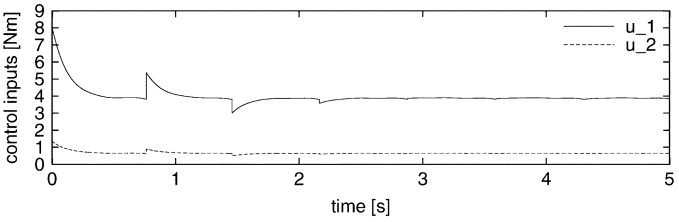

Fig. 13. Convergence of the control inputs.

control as a function of X_g, that is, to introduce a CoMJ formula. Let us consider the following condition:

$$\frac{\partial E}{\partial X_g} = -\zeta(E - E_d). \tag{34}$$

We then have to derive a solution which satisfies both conditions of (21) and (34). Based on the linearity of these equations, we can obtain the solution by adding the independent solutions of (21) and (34). Robust CoMJ formula then yields

$$\boldsymbol{Su}_{\rm vg} = (Mg\tan\phi - \zeta(E - E_d))\boldsymbol{J}_X(\boldsymbol{\theta})^T. \tag{35}$$

One way to investigate the orbital stability of a limit cycle is to study its fixed point in the Poincaré return map $\boldsymbol{x}_{k+1} = \boldsymbol{F}(\boldsymbol{x}_k)$ [5]. As a natural choice of the discrete state $\boldsymbol{x}_k$ for the Poincaré section, we can take the state at the transition instant, relative hip joint angle, and angular velocities at just after impact. In the case of steady walking, the relation $\boldsymbol{F}(\boldsymbol{x}^*) = \boldsymbol{x}^*$ holds where $\boldsymbol{x}^*$ is the equilibrium point of $\boldsymbol{x}_k$. Then, the discrete system expression can be obtained as

$$\delta\boldsymbol{x}_{k+1} = (\nabla\boldsymbol{F})\delta\boldsymbol{x}_k \tag{36}$$

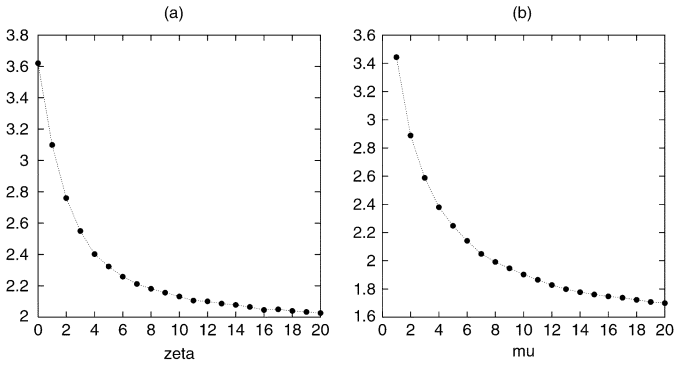

Fig. 14. Maximum singular value plot w.r.t. the adjustment parameters where $\phi = 0.0265$ rad.

where $\delta\boldsymbol{x}_k$ is a small perturbation around the limit cycle and $\nabla\boldsymbol{F}$ is the Jacobian (gradient) w.r.t. $\boldsymbol{x}^*$. The maximum singular value of $\nabla\boldsymbol{F}$ can be used to evaluate the robust performance, in other words, its smaller value means high-speed convergence of a cycle. Please see [1] for further details. Fig. 14(a) shows the change of the maximum singular value of $\nabla\boldsymbol{F}$ w.r.t. ζ. We can see that the maximum singular value decreases monotonically with the increase of ζ, which shows the effectiveness of the energy feedback control.

Next, we analyzed robust performance according to the torque distribution. For each method, we respectively use the CoMJ formula for the main term and the CTR formula for the energy feedback one and obtain the solution as follows:

$$\boldsymbol{Su}_{\rm vg} = Mg\tan\phi\boldsymbol{J}_X(\boldsymbol{\theta})^T - \begin{bmatrix}\mu+1\\-1\end{bmatrix}\frac{\zeta(E-E_d)\dot{X}_g}{(\mu+1)\dot{\theta}_1 - \dot{\theta}_2}. \tag{37}$$

Fig. 14(b) shows the numerical analysis result. The maximum singular value of $\nabla\boldsymbol{F}$ decreases monotonically with the increase of μ. This means that the stance leg side torque, which kicks a floor, is more important than the hip joint one to increase the robust stability.

B. Energy Efficiency

Now we analyze the energy efficiency of the controlled walking system. Let T s be the steady step period and p J/s the average input power, which is defined as

$$p := \frac{1}{T}\int_{0+}^{T^-}(|\dot{\theta}_1 u_1| + |(\dot{\theta}_1 - \dot{\theta}_2)u_2|)\,dt. \tag{38}$$

The average walking speed v m/s is also defined as

$$v := \frac{1}{T}\int_{0+}^{T^-}\dot{X}_g dt = \frac{\Delta X_g}{T} \tag{39}$$

where $\Delta X_g := X_g(T^-) - X_g(0^+)$ m is the steady value of the change of horizontal CoM position and is equal to the steady step length. Based on these definitions, the energy efficiency is defined as v/p m/J [13], [10]. This means the movable distance in the same energy supply and is a spatial criterion. Fig. 15 shows the result of walking speed v versus efficiency v/p by changing the virtual slope angle ϕ in (28). In this figure, v increases and v/p decreases monotonically with the increase of ϕ. There exists a tradeoff between v and v/p. For larger values of ϕ, the robot system exhibits period-doubling bifurcation [5].

We further consider the performances w.r.t. the torque distribution by using the CTR formula of (23). Fig. 16 shows the numerical results, where (a) v/p and (b) v w.r.t. μ correspond to three different values of virtual slope angle ϕ rad, respectively. We can see that both of them increase monotonically with the increase of μ and saturate each maximum value. In the following, we will consider this reason theoretically.

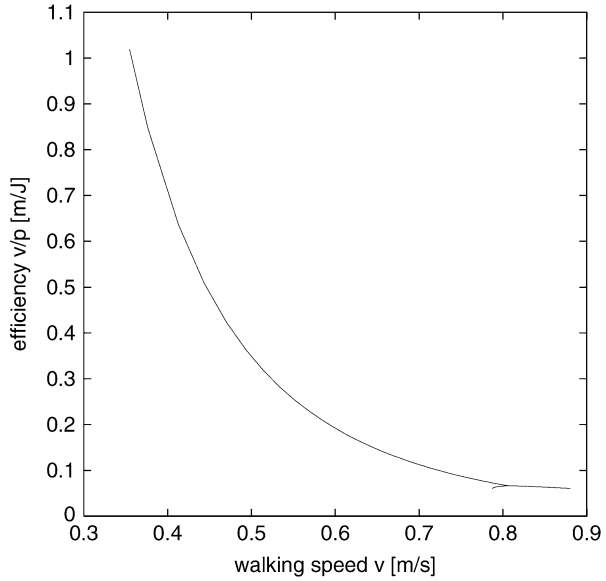

Fig. 15. v versus v/p of virtual passive dynamic walking.

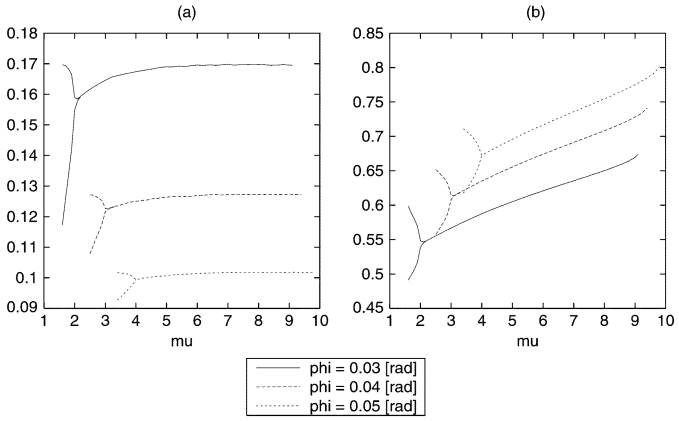

Fig. 16. Performance changes w.r.t. μ for $\phi = 0.03, 0.04$, and 0.05 rad.

Note that, for the definite integral of an absolute function to calculate p, the following relations hold:

$$p \geq \frac{1}{T}\int_{0+}^{T^-} |\dot{\theta}_1 u_1 + (\dot{\theta}_1 - \dot{\theta}_2)u_2|\, dt \tag{40}$$

$$= \frac{1}{T}\int_{0+}^{T^-} |\dot{E}|\, dt$$

$$\geq \frac{1}{T}\int_{0+}^{T^-} \dot{E}\, dt \tag{41}$$

$$= \frac{1}{T}\int_{0+}^{T^-} Mg\tan\phi \dot{X}_g dt$$

$$= \frac{Mg\tan\phi \Delta X_g}{T}. \tag{42}$$

The equality holds in (40) iff $\dot{\theta}_1 \geq 0$ and $\dot{\theta}_1 - \dot{\theta}_2 \geq 0$ because u_1 and u_2 are always positive during the swing phase under the assumption that the condition $(\mu+1)\dot{\theta}_1 - \dot{\theta}_2 > 0$ holds in (23). Since this paper does not treat the case that the system passes over the singular point of (23), u_1 and u_2 are always positive. In general, $\dot{\theta}_1 \geq 0$ holds, and $\dot{\theta}_1 - \dot{\theta}_2$ always becomes positive if μ is larger than a certain value. In order to verify this, we show their time evolutions in Fig. 17 where $\mu = 2.5$ and 8.0. This is because the larger μ causes larger weight of ankle torque control, and this leads acceleration of the CoM's velocity.

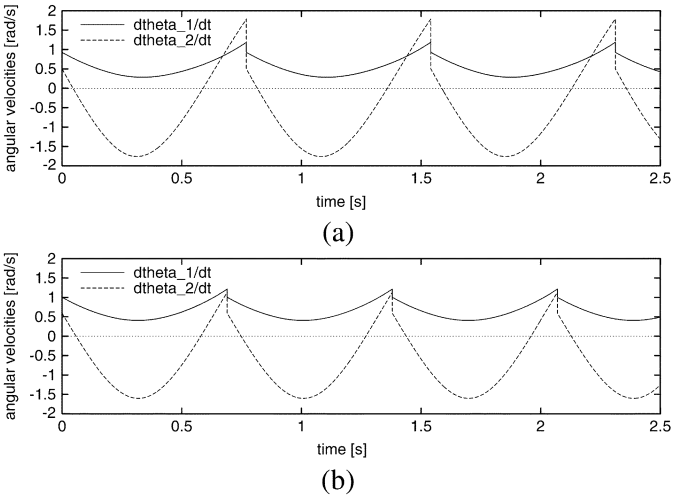

Fig. 17. Time evolutions of angular velocities for $\mu = 2.5$ and 8.0 where $\phi = 0.03$ rad. (a) $\mu = 2.5$, (b) $\mu = 8.0$.

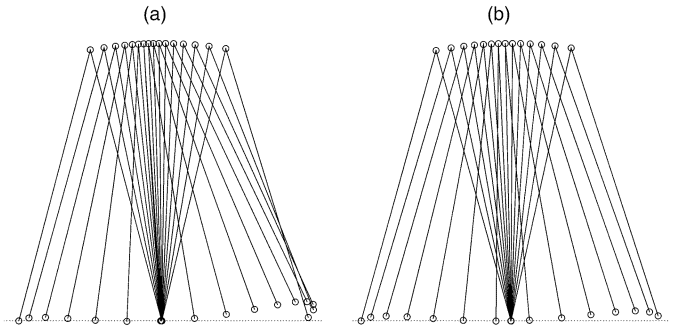

Fig. 18. Stick diagrams for $\mu = 2.5$ and 8.0 where $\phi = 0.03$ rad.

Fig. 18 shows the stick diagrams. We can see that a larger μ creates a smarter walking pattern without flinging up the swing leg wastefully.

The equality holds in (41) iff $\dot{E} \geq 0$. Therefore, monotonic mechanical energy restoration is found to be a necessary condition for energy-effective dynamic walking [1]. Furthermore, under the assumption that $\dot{X}_g \geq 0$, the following relation holds:

$$\int_{0+}^{T^-} \dot{E}\, dt = \int_{0+}^{T^-} \frac{\partial E}{\partial X_g}\dot{X}_g dt = \int_{X_g(0^+)}^{X_g(T^-)} \frac{\partial E}{\partial X_g} dX_g. \tag{43}$$

Therefore, monotonic energy restoration w.r.t. X_g is also found as a necessary condition because $dX_g \geq 0$.

Following (39) and (42), we can analytically obtain the relation

$$\frac{v}{p} \leq \frac{1}{Mg\tan\phi} \tag{44}$$

and the right-hand side is the maximum efficiency given by the solution of (22) which is strongly supported by Fig. 16(a). In the maximum efficiency case, we must further compare the walking speeds. Fig. 16(b) shows the simulation results of μ versus v. We can see that v monotonically increases with the increase of μ. Therefore, we can conclude that the CoMJ formula is not the optimal solution but rather the CTR formula with the maximum μ because it can provide the best spatial and time performance of a solution to (22), which means that *the active use of ankle torque achieves both increasing v and decreasing the ratio of p to v simultaneously*.

More general measure of efficiency is the specific resistance: p/Mgv, which is the output power in relation to the mass moved and the velocity attained. It is a dimensionless quantity [6]. In the case of

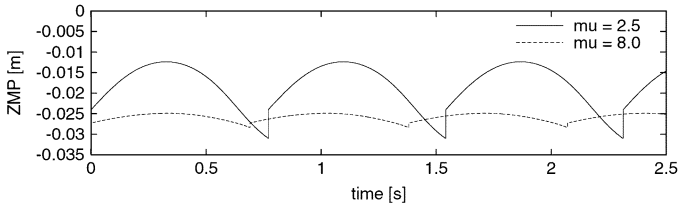

Fig. 19. Time evolutions of the ZMP for $\mu = 2.5$ and 8.0 where $\phi = 0.03$ rad.

virtual passive dynamic walking, following (44), we can obtain the relation

$$\frac{p}{Mgv} \geq \tan\phi. \tag{45}$$

The equality holds with the larger μ of CTR formula. Considering the range of ϕ, it can be said that the virtual gravity approach gives a higher performance for energy efficiency compared with the previous works.

The numerical analysis obtained in this section suggests that the motion of the stance leg kicking the floor is much more important than the hip joint control for energy-effective and robust dynamic walking. With the increase of μ, however, the ZMP condition becomes a serious problem. Fig. 19 shows the time evolutions of the ZMP where $\mu = 2.5$ and 8.0. Although in the case with large μ, the average magnitude of ZMP is larger, its range becomes narrow. This result implies that whether the ZMP condition is critical or not does not depend on the adjustment of μ but rather on the mechanical energy restoration orbit [1].

C. Discussion

The model of Fig. 1 is impossible to walk only by the hip joint torque only with $\mu = 0$. As shown in Fig. 16, the period-doubling bifurcation occurs for the smaller μ, and this implies the difficulty of gait generation. In this model, as mentioned, μ is about 6.0 in the case of the CoMJ formula [see (17)]. This is because the hip mass m_H is large and causes large ankle torque. If m_H does not exist, a stable limit cycle could be generated even if $\mu = 0$. Successful results with hip joint torque only reported so far do not have hip mass [10], [8].

On the other hand, the virtual gravity control gives the simplest trajectory for mechanical energy restoration and can produce a high-performance dynamic gait, but this cannot be concluded to be the optimal one. Search of the optimal energy trajectory is left as the future work. As mentioned above, so long as we use the CTR formula of (23), the influence of the ZMP condition is not serious. In the case when using other trajectories, for example, energy tracking control, it will become a serious problem as we have reported in [1]. Since quadruped robots can make closed link with floor, the control torques can be generated w.r.t. the body link and ZMP problem is released [12]. This is the essential difference between biped and multilegged robots. How to overcome the difficulty in the biped case then yields the main subject. One candidate solution is to use a torso. Fig. 20 shows a model of the compass-gait biped with a torso which can exert control torques u_1 and u_2 w.r.t. the torso. Although it is difficult to generate a stable limit cycle while balancing the torso, this subject is worth investigating to realize high performance dynamic walking. In addition, in this case the average input power p is defined as

$$p := \frac{1}{T}\int_{0^+}^{T} \left(|(\dot\theta_1 - \dot\theta_3)u_1| + |(\dot\theta_2 - \dot\theta_3)u_2|\right) dt \tag{46}$$

and is different from (38) of the model in Fig. 1. As can be seen from this example, an optimal solution for a model is not necessarily the optimal one for the other models because the criterion differs according to the robot's structures.

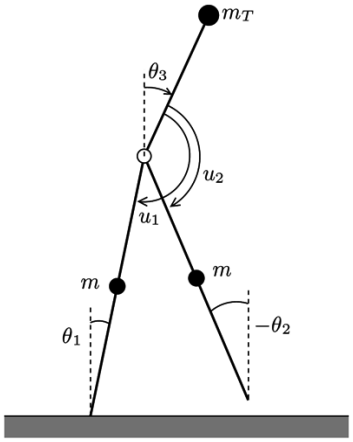

Fig. 20. Compass-gait biped robot with a torso.

VII. Conclusion and Future Works

In this paper, gait generation mechanisms in passive dynamic walking have been investigated from the mechanical energy point of view, and the biped gait generation problem has been formulated by deriving an indeterminate equation of the control input. As solutions of this indeterminate equation, we proposed a robust control design technique utilizing the characteristic of the mechanical energy behavior. The validation and control performances of the proposed methods have been confirmed throughout numerical simulations. The condition for the maximum efficiency has also been clarified theoretically.

Virtual gravity yields the simplest mechanical energy orbit of (21) which gives good condition of ZMP. Further study on the general case of the energy reference trajectories is necessary. A ZMP problem may arise, and how to overcome it will be the subject for the future study. As mentioned in the previous section, the consideration of a torso seems to be a worthwhile subject to investigate. In addition, neglecting joint viscosity is also an important problem to be investigated for practical use. Although some problems are left unsolved, the authors think that the properties given in this paper are important for high-performance dynamic biped gait generation.

Appendix A
On the Torque Transformation

This appendix explains the detailed mechanism of torque transformation. Denote the positions of hip, stance leg, and swing leg as $\mathrm{P}_H, \mathrm{P}_1$, and P_2, respectively. Then, time derivative of the positions w.r.t. the origin O yield

$$\frac{d}{dt}\overrightarrow{\mathrm{OP}_H} = \boldsymbol{J}_H(\boldsymbol{\theta})\dot{\boldsymbol{\theta}} \tag{47}$$

$$\frac{d}{dt}\overrightarrow{\mathrm{OP}_1} = \boldsymbol{J}_1(\boldsymbol{\theta})\dot{\boldsymbol{\theta}} \tag{48}$$

$$\frac{d}{dt}\overrightarrow{\mathrm{OP}_2} = \boldsymbol{J}_2(\boldsymbol{\theta})\dot{\boldsymbol{\theta}} \tag{49}$$

respectively, and their Jacobians can be obtained as

$$\boldsymbol{J}_H(\boldsymbol{\theta}) = \begin{bmatrix} l\cos\theta_1 & 0 \\ -l\sin\theta_1 & 0 \end{bmatrix} \tag{50}$$

$$\boldsymbol{J}_1(\boldsymbol{\theta}) = \begin{bmatrix} a\cos\theta_1 & 0 \\ -a\sin\theta_1 & 0 \end{bmatrix} \tag{51}$$

$$\boldsymbol{J}_2(\boldsymbol{\theta}) = \begin{bmatrix} l\cos\theta_1 & -b\cos\theta_2 \\ -l\sin\theta_1 & b\sin\theta_2 \end{bmatrix}. \tag{52}$$

On the other hand, the affected force at each point by virtual gravity is obtained as

$$\boldsymbol{f}_H = \begin{bmatrix} m_H g \tan\phi \\ 0 \end{bmatrix}, \quad \boldsymbol{f}_1 = \boldsymbol{f}_2 = \begin{bmatrix} mg \tan\phi \\ 0 \end{bmatrix}.$$

From the above equations, the equivalent transformed torques are obtained as follows:

$$\boldsymbol{S}\boldsymbol{u}_{\mathrm{vg}} = \boldsymbol{J}_H(\boldsymbol{\theta})^T \boldsymbol{f}_H + \boldsymbol{J}_1(\boldsymbol{\theta})^T \boldsymbol{f}_1 + \boldsymbol{J}_2(\boldsymbol{\theta})^T \boldsymbol{f}_2. \tag{53}$$

Equation (12) is a detailed expression of (53), and (9) can be obtained easily from (12) by replacing the angle component as $\theta_1 \rightarrow \theta_1 - \phi$ and $\theta_2 \rightarrow \theta_2 - \phi$, and the gravity component as $g \tan\phi \rightarrow g \sin\phi$, respectively.

ACKNOWLEDGMENT

The authors wish to thank Dr. A. Goswami, Honda R&D Americas, Inc., for giving them many useful comments on the virtual gravity concept and its physical interpretation.

REFERENCES

[1] F. Asano, M. Yamakita, N. Kamamichi, and Z.-W. Luo, "A novel gait generation for biped walking robots based on mechanical energy constraint," *IEEE Trans. Robot. Autom.*, vol. 20, no. 3, pp. 565–573, Jun. 2004.

[2] F. Asano and M. Yamakita, "Virtual gravity and coupling control for robotic gait synthesis," *IEEE Trans. Syst., Man, Cybern. A*, vol. 31, no. 6, pp. 737–745, Nov. 2001.

[3] F. Asano, Z. W. Luo, and M. Yamakita, "Some extensions of passive walking formula to active biped robots," in *Proc. IEEE Int. Conf. Robot. Autom.*, vol. 4, 2004, pp. 3797–3802.

[4] A. Goswami, B. Espiau, and A. Keramane, "Limit cycles in a passive compass gait biped and passivity-mimicking control laws," *Auton. Robots*, vol. 4, no. 3, pp. 273–286, 1997.

[5] A. Goswami, B. Thuilot, and B. Espiau, "Compass-like biped robot Part I: Stability and bifurcation of passive gaits," INRIA, Res. Rep. 2613, 1996.

[6] P. Gregorio, M. Ahmadi, and M. Buehler, "Design, control, and energetics of an electrically actuated legged robot," *IEEE Trans. Syst., Man, Cybern. B*, vol. 27, no. 4, pp. 626–634, Aug. 1997.

[7] S. Kajita, T. Yamaura, and A. Kobayashi, "Dynamic walking control of a biped robot along a potential energy conserving orbit," *IEEE Trans. Robot. Autom.*, vol. 8, no. 4, pp. 431–438, Aug. 1992.

[8] R. Q. van der Linde, "Actively controlled ballistic walking," in *Proc. IASTED Int. Conf. Robot. Applicat.*, 2000, pp. 135–142.

[9] T. McGeer, "Passive dynamic walking," *Int. J. Robot. Res.*, vol. 9, pp. 62–82, 1990.

[10] K. Ono, R. Takahashi, and T. Shimada, "Self-excited walking of a biped mechanism," *Int. J. Robot. Res.*, vol. 20, no. 12, pp. 953–966, 2001.

[11] K. Ono, T. Furuichi, and R. Takahashi, "Self-excited walking of a biped mechanism with feet," *Int. J. Robot. Res.*, vol. 23, no. 1, pp. 55–68, 2004.

[12] K. Osuka and Y. Saruta, "Development and control of new legged robot QUARTET III—From active walking to passive walking," in *Proc. Int. Conf. Intell. Robots Syst.*, vol. 2, 2000, pp. 991–995.

[13] J. E. Pratt and G. A. Pratt, "Exploiting natural dynamics in the control of a planar bipedal walking robot," in *Proc. 36th Annu. Allerton Conf. Commun., Control, Comput.*, 1998, [CD-ROM].

[14] A. Sano and J. Furusho, "Realization of natural dynamic walking using the angular momentum information," in *Proc. IEEE Int. Conf. Robot. Autom.*, 1990, pp. 1476–1481.

[15] M. W. Spong, "Passivity-based control of the compass gait biped," in *Proc. World Congr. IFAC*, 1999, pp. 19–23.

Electroencephalogram-Based Control of an Electric Wheelchair

Kazuo Tanaka, Kazuyuki Matsunaga, and Hua O. Wang

***Abstract*—This paper presents a study on electroencephalogram (EEG)-based control of an electric wheelchair. The objective is to control the direction of an electric wheelchair using only EEG signals. In other words, this is an attempt to use brain signals to control mechanical devices such as wheelchairs. To achieve this goal, we have developed a recursive training algorithm to generate recognition patterns from EEG signals. Our experimental results demonstrate the utility of the proposed recursive training algorithm and the viability of accomplishing direction control of an electric wheelchair by only EEG signals.**

***Index Terms*—Direction control, electric wheelchair, electroencephalogram (EEG)-based control, recursive training algorithm.**

I. INTRODUCTION

There are numerous interfaces and communication methods between human and machines. A typical human–machine interface is to utilize input devices such as keyboards, a mouse, or joysticks. Recently, a number of biological signals such as electromyogram (EMG) [1] and electroencephalogram (EEG) [2] have been employed as hands-free interfaces to machines (e.g., see [3]–[5]). In particular, the so called brain–computer interface (BCI) [6]–[10] has received significant attention. The BCI is a system that acquires and analyzes neural (brain) signals with the goal of creating a direct high-bandwidth communication channel between the brain and the computer. Such systems are envisioned to have huge potentials for a wide ranging areas of research and applications such as brain (neural) signal acquisition and processing, bioengineering, and understanding the underlying neuroscience, to name a few. For systems and controls research, advances on brain–machine interfaces offer intriguing opportunities and challenges, for instance, brain control of machines.

There have been several studies using hands-free inputs in controlling machines through brainwaves. For example, speed and direction control of a small mobile robot using brainwaves and small facial muscular movements was reported in [11]. In this study, beta wave amplitude of EEG, jaw clench, and eye muscle signal [electrooculogram (EOG)] are used to control the speed, forward/backward switching, and the direction, respectively. In the system of [11], it is clear that the primary control signals for the mobile robot are jaw clench and eye muscle signals. The brainwaves are limited to controlling the speed of the mobile robot. The control objective was to move the mobile robot but without any specified or desired target positions. The paper did not report the success and/or failure rates of reaching the target positions. Bare [12] and Felzer [13] investigated wheelchair control using EOG and EMG, respectively. To the best of our knowledge, there has been no report of wheelchair control using only EEG in the literature.

In this paper, we investigate and demonstrate direction control of an electric wheelchair using only EEG signals. In addition, we present

Manuscript received January 14, 2004; revised August 17, 2004. This paper was recommended for publication by Associate Editor F. Y. Wang and Editor F. Park upon evaluation of the reviewers' comments.

K. Tanaka and K. Matsunaga are with the Department of Mechanical Systems and Intelligent Systems, The University of Electro-Communications, Tokyo 182-8585, Japan (e-mail: ktanaka@mce.uec.ac.jp; matunaga@rc.mce.uec.ac.jp).

H. O. Wang is with the Department of Aerospace and Mechanical Engineering, Boston University, Boston, MA 02215 USA (e-mail: wangh@bu.edu).

Digital Object Identifier 10.1109/TRO.2004.842350